

# Optimization of tumor virotherapy with recombinant measles viruses

Željko Bajzer

Biomathematics Resource  
Dept. of Biochemistry and Molecular Biology  
Mayo Clinic College of Medicine  
Rochester, MN 55905, USA

Thomas Carr

Department of Mathematics  
Southern Methodist University  
Dallas, TX 75275, USA

David Dingli

Division of Hematology  
Mayo Clinic College of Medicine  
Rochester, MN 55905, USA

Krešimir Josić

Department of Mathematics  
University of Houston  
Houston, TX 77204-3008, USA

May 17, 2007

## Abstract

Recombinant viruses based on the vaccine strain of measles virus have potent and selective activity against a wide range of tumors. Successful tumor therapy with these viruses (virotherapy) depends on efficient infection of tumor cells by the virus. Infected cells express viral proteins that allow them to fuse with neighboring cells to form syncytia. Infection halts tumor cell replication and the syncytia ultimately die. Moreover, infected cells may produce new virus particles that proceed to infect additional tumor cells. The outcome of virotherapy depends on the dynamic interactions between the uninfected tumor cells, infected cells and the virus population. We present a model of tumor and virus interactions based on the phenomenologically established interactions between the three populations. Other similar models proposed in the literature are also discussed. The model parameters are obtained by fitting the model to experimental data. We discuss equilibrium states and explore by simulations the impact of various initial conditions and perturbations of the system in an attempt to achieve tumor eradication. We show that the total dose of virus administered and the rate at which the

tumor growth play determining roles on the outcome. If tumor growth can be slowed, the minimal dose of virus needed for curative therapy can be reduced substantially. An interesting prediction of the model is that virotherapy is more effective on larger tumors when deceleration of growth occurs.

## 1 Introduction

The majority of hematopoietic neoplasms remain incurable with currently available therapies. For example, multiple myeloma (MM), has a median survival of 3 to 4 years despite the availability of high-dose therapy with stem cell transplantation and the introduction of novel agents such as thalidomide and bortezomib [1]. Thus there is an urgent need for novel therapeutic modalities for these disorders. Over the last few years, engineered viruses (both DNA and RNA based) have been introduced as potential cancer therapeutic agents [2, 3]. Several trials have been performed with replication selective adenoviruses in head and neck cancer [4] and metastatic colon carcinoma [5, 6] while Newcastle disease virus has been given to patients with various tumor types [7]. The use of viruses for tumor therapy introduces several new concepts in the field of therapeutics since an underlying premise of tumor therapy is that the infected tumor cells become factories that generate new virus particles that infect more tumor cells in a series of waves [2]. This introduces the concept of population dynamics and the outcome of such therapy depends in a complex way on the interactions between the population of virus and tumor cells [8, 9, 10, 11, 12].

Our work has centered on the use of engineered viruses, derived from the Edmonston vaccine strain of measles virus (MV-Edm). The vaccine strain was chosen as a therapeutic platform because of anecdotal reports of resolution of Burkitt's lymphoma in patients who acquired wild type measles virus infection. Moreover, the vaccine has been given to more than a billion people with an excellent safety record. MV-Edm and derivative viruses obtained by virus engineering have potent and selective oncolytic activity against a wide variety of human tumors including non-Hodgkin lymphoma [13], multiple myeloma [14], ovarian carcinoma [15], glioma [16] and breast carcinoma [17] while they leave normal tissues unharmed.

MV infection starts when the viral hemagglutinin protein (H) binds to its receptor on target cells. The H protein displayed by wild type measles virus preferentially binds to CD150 (also known as SLAM) [18] while the H protein of MV-Edm preferentially interacts with CD46 [18]. Most tumor cells over-express CD46 [19, 20] and this is thought to be one of the mechanisms behind the selective tropism of these viruses for tumor cells. Binding of the H protein with its cognate receptor, induces conformational changes in the fusion (F) protein which in turn triggers membrane fusion between the virus particle and the target cell. The functional separation of target cell binding (via H) and fusion (via F) in MV also facilitated re-targeting of the virus to specific tumors by modification of the viral H protein [21, 22, 23, 24]. Protein engineering has also led to complete ablation of H binding to the known viral receptors (CD46 and CD150w) so that fully re-targeted viruses that only infect tumor cells of interest have been generated [25, 26, 27]. In addition, MV vectors have been modified to allow non-invasive monitoring of viral gene expression by the secretion of

the biologically inert soluble peptides CEA (MV-CEA) and human chorionic gonadotrophin (hCG, MV-hCG) [28]. More recently, MV-Edm has been modified to induce expression of the thyroidal sodium iodide symporter (NIS, MV-NIS) in infected cells to enable non-invasive imaging of the biodistribution and replication of the virus in vivo [29, 30].

Although MV based vectors have potent oncolytic activity, some tumors are not eliminated in vivo. Studies using MV-CEA show that although the virus efficiently infects and propagates in these tumors, the latter may persist [15, 29, 31]. This highlights the dynamic interplay between viral replication, tumor cell growth and the death rate of infected tumor cells [8, 9, 10, 11, 12, 32, 33]. In this respect, MV-NIS has an advantage over the parent virus since it can be combined with beta particle emitting isotopes such as  $^{131}\text{I}$ . The electrons emitted during isotope decay have a macroscopic path length and can destroy uninfected tumor cells with a significant bystander effect [29, 34, 35].

Measles virus can control tumor growth by at least two mechanisms. Infected cells express the viral H and F proteins and can interact with neighboring cells with the result that the cells fuse together. Spread of cell-to-cell fusion leads to the formation of syncytia that ultimately die, usually after a few days [14, 15]. In addition, once infected cells die, they may release free virus particles that can infect surrounding cells. Moreover, infected cells stop replicating and do not contribute to further tumor growth.

The success of tumor virotherapy depends on infection of tumor cells that serve as sites for virus amplification. Once the virus is released from infected cells, the new particles can infect additional tumor cells. Thus, the virus propagates through the tumor in a series of 'waves' [2]. The interactions between the tumor and virus populations are complex and understanding their dynamics requires mathematical modeling. There has already been considerable work on modeling these interactions [8, 9, 10, 11, 33, 32, 36].

In the following, we describe our model of tumor and virus interactions that takes into consideration both virus production and spread of the infection between cells. We utilize the model to evaluate various therapeutic scenarios and to test whether curative therapy is possible with virus alone or virus in combination with other agents. Patients with advanced hematological cancer are usually immunosuppressed and hence the smallest dose of virus as well as timing of therapy may be critical for an optimal response. It seems logical to try and determine the smallest possible dose of virus that can be associated with a cure, given that this will probably be associated with the lowest risk of complications. In the following, we address several critical questions pertaining to tumor therapy including:

- 1) Is the initial tumor burden important for the outcome of therapy?
- 2) Is cure possible with a therapeutically achievable dose of virus?
- 3) Can therapy be optimized such that the dose of virus is minimized?
- 4) Does dose scheduling play an important role on the outcome of therapy?

We are aware of the importance of the immune response to measles virus and its potential adverse consequences on the outcome of therapy. This is a current focus of our research

efforts. The model we have developed is fitted to data obtained for the growth of myeloma tumor xenografts implanted in immunocompromised mice and treated with a recombinant measles virus. Given that these mice do not have an immune response we will not consider the immune system further.

## 2 Mathematical model of virotherapy

Modeling the effects of any therapy on tumor growth requires a model for the growth of the untreated tumor. Usually, untreated tumor growth is reliably described by the Gompertz function [37, 38, 39, 40], yet for some tumors the more general Bertalanffy-Richards (or generalized logistic) model is required to describe data adequately [41, 12]. We use the Bertalanffy-Richards model given by

$$y' = (g/\varepsilon)y[1 - (y/K)^\varepsilon], \quad \varepsilon > 0, \quad y(0) = y_0, \quad (1)$$

where  $y(t)$  is the size of the tumor cell population,  $r = g/\varepsilon > 0$  is the effective growth rate constant and  $K > 0$  is the carrying capacity. We note that in the limit  $\varepsilon \rightarrow 0$  the Bertalanffy-Richards and Gompertz models are equivalent [42, 43]. The solution of equation (1) can be written in an explicit form [42, 43, 44]

$$y(t) = y_0[f^\varepsilon + (1 - f^\varepsilon)e^{-gt}]^{-1/\varepsilon}, \quad \text{where } f = y_0/K. \quad (2)$$

To model the effects of virotherapy we have to consider the dynamics of at least three interacting populations [9, 12]:

- $y(t)$  – uninfected tumor cells,
- $x(t)$  – virus-infected tumor cells, and
- $v(t)$  – free infectious virus particles.

A graphical representation of the model is given in Fig. 1.

As noted in the Introduction, the infection spreads in tumor cells either by a productive encounter of one free virus particle with one uninfected cell, or by an encounter of an infected cell (expressing the viral F and H proteins) with an uninfected cell. In the latter case two cells fuse to form a syncytium that continues to spread acquiring new surrounding cells. Thus, the rate at which the population of uninfected cells is depleted is given by the sum  $\kappa y(t)v(t) + \rho y(t)x(t)$ , where  $\kappa > 0$  and  $\rho \geq 0$  are corresponding rate constants.

Uninfected cells are assumed to be proliferating according to the Bertalanffy-Richards model. Infected cells most probably do not proliferate [45], but are assumed to be dying at the effective rate  $\delta x(t)$  (Fig. 1). The rate constant  $\delta$  may include the rate constant of apoptotic death ( $a > 0$ ) and possibly a very small rate constant for proliferation ( $p$ ), so that  $\delta = a - p \geq 0$ .

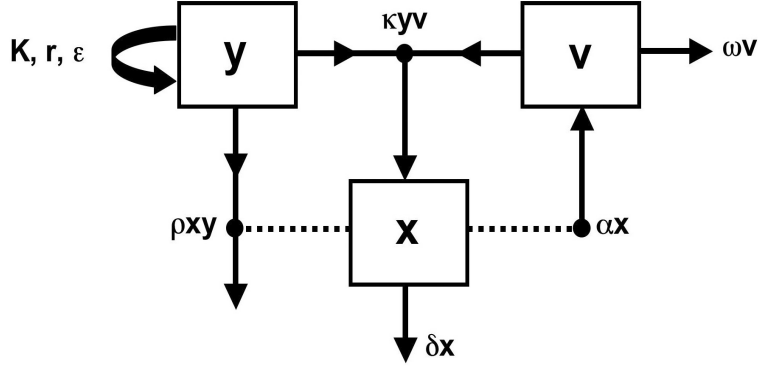


Figure 1: Schematic diagram of the proposed model for virotherapy. Here  $y$  denotes the populations of uninfected cells. Proliferation of these cells is described by an effective proliferation rate  $r$ , carrying capacity  $K$  and parameter  $\varepsilon$  which characterizes the shape of the sigmoidal growth curve. Populations of infected cells and virus are denoted by  $x$  and  $v$  respectively. Indicated rates of first and second order are explained in the text. Solid line arrows signify population influx or depletion, while dotted lines indicate that corresponding rates depend on population  $x$ .

The population of free virus particles can grow when infected cells (including syncytia) burst and release virions that have replicated within the cell. Thus the rate of free virus replication can be modeled by  $\alpha x$  where  $\alpha \geq 0$  is the corresponding rate constant. Finally, the rate of free virus elimination is modeled by the sum  $\kappa y(t)v(t) + \omega v(t)$  (Fig. 1). The first term in the sum corresponds to the rate at which virus particles enter uninfected cells. Note that we assume that one virus particle infects one cell. These particles are incapable of infecting further cells and are no longer part of the free virus population. The term  $\omega v(t)$ ,  $\omega \geq 0$  represents a rate of elimination of free virus particles by other causes including non-specific binding and generation of defective interfering particles.

With these assumptions about rates, the virotherapy model can be represented by the following system of differential equations:

$$\begin{aligned}
 y' &= ry[1 - (y + x)^\varepsilon / K^\varepsilon] - (\kappa yv + \rho yx), & y(0) &= y_0, \\
 x' &= \kappa yv - \delta x, & x(0) &= 0, \\
 v' &= \alpha x - (\kappa yv + \omega v), & v(0) &= v_0.
 \end{aligned} \tag{3}$$

The tumor is assumed to have grown to size  $y_0$  when a single dose of virus  $v_0$  is injected at time  $t = 0$ . The term  $(y + x)^\varepsilon / K^\varepsilon$  ensures that the tumor cannot grow beyond carrying capacity  $K$ . The mathematical proof of this property of system (3) is analogous to the proof given in Appendix A of [12].

The rate term  $\rho yx$ , which describes one possible way of infection, does not appear in the equation for  $x'$  because no new infected cell was generated in that encounter. Rather, an uninfected cell became fused with an infected cell, or with an already formed syncytium. Therefore, the population  $x(t)$  is assumed to consist of single infected cells and syncytia.

Experimental evidence suggests that infection is mostly due to such fusion with infected cells, rather than by free virus infection, which suggests that  $\kappa \ll \rho$  (see [15, 29] and Section 4). Although the rate constant  $\kappa$  in (3) may be small compared to  $\rho$ , it still should not be completely negligible. Namely, if  $\kappa = 0$ , the model (3) breaks down because  $x(t)$  may become negative. Thus we have to assume  $\kappa > 0$ , or reduce the model to the following:

$$\begin{aligned} y' &= ry[1 - (y + x)^\varepsilon/K^\varepsilon] - \rho yx, & y(0) &= y_0 > 0, \\ x' &= -\delta x, & x(0) &= x_0 > 0, \end{aligned} \quad (4)$$

In this simplified model it is assumed that there is an initial, fast free virus infection. This yields a number  $x_0$  of infected cells which then infect other cells by fusion. This model did not fit the existing data (Section 4) and will not be considered further.

The proposed model (3) is different from some previous models of virotherapy based on population dynamics [8, 9, 10, 11, 12, 32, 46]. Wodarz [9] has proposed and discussed a model in which  $\rho = 0$ ,  $\varepsilon = 1$  and the  $\kappa yv$  term in the equation for  $v'$  is absent:

$$\begin{aligned} y' &= ry[1 - (y + x)/K] - dy - \kappa yv, \\ x' &= \kappa yv - \delta x, \\ v' &= \alpha x - \omega v. \end{aligned}$$

Here the term  $dy$  models the death rate of uninfected cells. In our model (3) this term is not included because it is redundant. Formally one can write:

$$ry[1 - (x + y)^\varepsilon/K^\varepsilon] - dy = \tilde{r}[1 - (x + y)^\varepsilon/\tilde{K}^\varepsilon]$$

where  $\tilde{r} = r - d$ ,  $\tilde{K}^\varepsilon = (r - d)K^\varepsilon/r$ .

In a previous attempt to model the dynamics of infected and uninfected tumor cells, Wodarz ([8, 46]) included the infection term  $\beta yx$ , but neglected the dynamics of the free virus population. He considered the following model equations:

$$\begin{aligned} y' &= ry[1 - (x + y)/K] - dy - \beta xy \\ x' &= \beta xy + sx[1 - (x + y)/K] - \delta x \end{aligned} \quad (5)$$

Here it is assumed that both populations proliferate, although infected cells are not likely to proliferate [45]. The term  $\beta xy$  in equation (5) implicitly models the spread of virus and it is conceptually different from our term  $\rho xy$  representing the specific rate of infection via formation of syncytia.

Following Wodarz [9], in our previous model [12] we have not included the  $\rho xy$  term. Also not included was the  $\kappa yv$  term in the equation for  $v'$ . However, this term could be important, because in its absence the free virus particle count is not conserved. The models described in [10, 11, 33, 32] are more complex (and probably more realistic) spatio-temporal models; however they do not include the term analogous to  $\kappa yv$  in the equation for the virus population.

Population dynamics models, such as (3), are generally realistic when a population consists of many individuals. The goal of therapy is to reduce the total number of tumor cells, given by  $u(t) = x(t) + y(t)$ , to zero. However, due to the uniqueness of solutions, this goal can never be achieved in ordinary differential equations models of the type described here. We consider the tumor effectively eradicated if  $u(t) < 1$  is achieved at some finite time smaller or equal to the maximal lifetime of a mouse taken to be 1000 days. Also, if the tumor burden is below a detectable amount by 1000 days, the therapy is deemed successful. A tumor consisting of less than  $10^6$  cells (or approximately  $1 \text{ mm}^3$ ) is considered to be undetectable. The model may not be realistic when the number of tumor cells (or virus particles) is very small, so in some ways the lowest limit of 1 cell (or virus particle) is artificial. Yet, it can be used to estimate when the ultimate goal of virotherapy is achieved, i.e. when the tumor cell population is eliminated and there is no more free virus present.

### 3 Analysis of equilibria

The stable states of system (3) which are approached as  $t \rightarrow \infty$  represent the outcome of therapy, if the tumor burden  $x(t) + y(t)$  has not been reduced to a level below 1 cell at some finite time. Simulations suggest that for physiologically relevant parameters, all such states are equilibria. We therefore begin by characterizing the fixed points of the model and analyzing their stability.

In most parameter regimes there are three equilibrium points of system (3). The desired outcome of therapy corresponds to the equilibrium point at the origin:

$$y_1 = 0, \quad x_1 = 0, \quad v_1 = 0, \tag{6}$$

This is an unstable point for biologically relevant parameters. The Jacobian of the system for this point has the eigenvalues

$$\lambda_1 = r > 0, \quad \lambda_2 = -\delta < 0, \quad \lambda_3 = 0.$$

The unstable manifold of this equilibrium is the  $y$ -axis. This instability is a consequence of the assumptions made in the model: In the absence of the virus, the number of infected cells  $x$  will remain at 0, solutions will remain on the  $y$  axis and grow according to the Bertalanffy-Richards model.

In the absence of therapy, or if therapy fails, the tumor eventually grows to its maximal size. This is represented by the equilibrium point

$$y_2 = K, \quad x_2 = 0, \quad v_2 = 0. \tag{7}$$

The Jacobian of the system for this point has eigenvalues

$$\lambda_1 = -r\varepsilon/K < 0, \quad \lambda_{2,3} = -\delta - \kappa K - \omega \pm \sqrt{(\delta + \kappa K + \omega)^2 - 4q} \tag{8}$$

where

$$q = (\alpha - \delta)\kappa K - \delta\omega.$$

All eigenvalues are real for biologically relevant parameters. In case  $q < 0$  all eigenvalues are negative and the equilibrium is stable. When  $q > 0$  it follows from (8) that  $\lambda_2 > 0$  and the equilibrium is unstable. In the unlikely case that  $q = 0$  it follows  $\lambda_2 = 0$  and stability is determined by higher order terms.

Partial success of therapy is represented by the equilibrium point:

$$y_3 = \frac{\delta\omega}{(\alpha - \delta)\kappa}, \quad x_3 = \frac{1}{c} \left[ 1 - \left( \frac{x_3 + y_3}{K} \right)^\varepsilon \right], \quad v_3 = \frac{\alpha - \delta}{\omega} x_3, \quad (9)$$

where

$$c = \frac{\kappa(\alpha - \delta)}{r\omega} + \frac{\rho}{r}.$$

As discussed in the previous section  $x(t) + y(t) \leq K$ . Therefore, at this equilibrium point  $y_3 < K$ , since  $y_3 = K$  corresponds to the equilibrium point of complete therapy failure.

For biologically relevant parameters, non-negative values of  $y_3$  and  $v_3$  are obtained only for  $\alpha > \delta$ . In this case  $c > 0$ , and it is easy to show that equation (9) has a unique solution for  $x_3$ . Indeed, let us denote by  $\psi(\xi)$  the function

$$\psi(\xi) = [(\xi + y_3)/K]^\varepsilon + c\xi - 1.$$

This is a continuous function on the interval  $[0, K - y_3]$  and  $\psi(0) = (y_3/K)^\varepsilon - 1 < 0$ , while  $\psi(K - y_3) = c(K - y_3) > 0$ . Therefore  $\psi(\xi)$  has zero within this interval, i.e., there exists at least one  $x_3 \in [0, K - y_3]$  which solves the nonlinear equation (9). Furthermore, this solution is unique, because if we assume two different solutions  $\xi_1$  and  $\xi_2$ , then  $\psi(\xi_1) - \psi(\xi_2) = 0$  and therefore

$$[(\xi_1 + y_3)/K]^\varepsilon - [(\xi_2 + y_3)/K]^\varepsilon = -c(\xi_1 - \xi_2).$$

Both  $\xi_1 > \xi_2$  and  $\xi_1 < \xi_2$  lead to a contradiction and therefore  $\xi_1 = \xi_2$ . Thus, the equilibrium (9) is uniquely defined for all biologically relevant parameters. The only exception are the cases  $\omega = 0$  and  $\alpha = \delta$ , when (9) does not exist, and only (6) and (7) are relevant. The significance of equilibrium (9) is that it offers a permanent reduction of tumor burden if therapy fails to eliminate tumor cells at some finite time.

Finding the eigenvalues of the Jacobian at the equilibrium point  $(y_3, x_3, v_3)$  leads to solving a cubic equation. The Routh-Hurwitz criterion [47] for the solutions indicates that for some combinations of model parameters all the solutions can have negative real parts and therefore the equilibrium point can be stable. However, since equation for  $x_3$  cannot be analytically solved, the conclusion about stability has to be reached by numerical calculations for the specific parameter values.

In the next section it is shown that experimental data for myeloma tumor size in mice under virotherapy with MV-NIS are consistent with  $\alpha = \omega = 0$ . This implies that approximately no free virus is being produced in vivo and the therapeutic effect of virotherapy is only due to cell-to-cell fusion and syncytium formation. Also, this singular model implies that the free virus is not decreased due to elimination or inactivation. In this case the equilibrium corresponding to successful therapy (6) and that corresponding to therapy failure (7) remain unchanged in location and stability.

In addition to the equilibria (6, 7) discussed above there is now a line of fixed points given by

$$L = \{(y, x, v) : y_3 = x_3 = 0, \text{ and } v = \bar{v} \text{ is arbitrary}\}. \quad (10)$$

These equilibria represent the situation when the tumor is eradicated, but there is a residual virus population  $\bar{v}$ . The size of this residual population depends on initial conditions. The Jacobian at each fixed point (10) has the eigenvalues

$$\lambda_1 = 0, \quad \lambda_2 = -\delta < 0, \quad \lambda_3 = r - \kappa\bar{v}. \quad (11)$$

The eigenvalue  $\lambda_1$  corresponds to an eigenvector parallel with  $L$ , and the stability of points on  $L$  is determined by the sign of  $\lambda_2$  and  $\lambda_3$ . Therefore all points satisfying

$$\bar{v} < \frac{r}{\kappa}$$

are stable, and those satisfying the opposite inequality are unstable. As shown in Fig. 2, the point  $(0, 0, r/\kappa)$  lies on a separatrix between the basin of attraction of the line, and the basin of attraction of the equilibrium  $(K, 0, 0)$  representing therapy failure. We note that the line given by (10) is invariant for any parameter values, however in the case that  $\alpha$  and  $\omega$ , are small and positive which still might be consistent with our data (see next Section),  $L$  is no longer attracting. We discuss this further in Section 5.

## 4 Model validation and parameter estimation

The proposed model (3) was validated by least-square fits to available experimental data obtained for multiple myeloma induced in SCID mice [29]. These data include the tumor growth curve without treatment, and the growth curve when virotherapy is introduced on day 15. Tumor size was measured as volume (in  $mm^3$ ), while our model considers population of cells. In the following we will assume that  $1 mm^3$  corresponds to  $10^6$  cells and we will consider cell and virion populations  $y, x, v$  as expressed in units of  $10^6$ .

The model was validated and parameters estimated by using the weighted non-linear least squares method. Weighting factors were chosen as  $1/\sigma_i^2$ , where  $\sigma_i$  is the experimentally determined standard deviation for the  $i$ -th data point. Technically, least-squares fitting was conveniently performed in MLAB ( MD, <http://www.civilized.com>, Civilized Software Inc., Bethesda, MD), but in cases where the minimum was difficult to find, we used our minimizer [48] in conjunction with a custom made ODE solver.

In the case of untreated tumor the fitting was relatively simple, as the analytic form of the solution is known (see equation (2)). A good fit was obtained with the exponent  $\varepsilon \approx 1.65$  rather than  $\varepsilon \approx 0$ , which would imply that growth follows the Gompertz function (see Fig. 3 for parameter estimates). By using model selection criteria we have shown that the generalized model with  $\varepsilon \approx 1.65$  more adequately fits the growth data for untreated tumor than both the Gompertz and the logistic model ( $\varepsilon = 1$ ) [12].

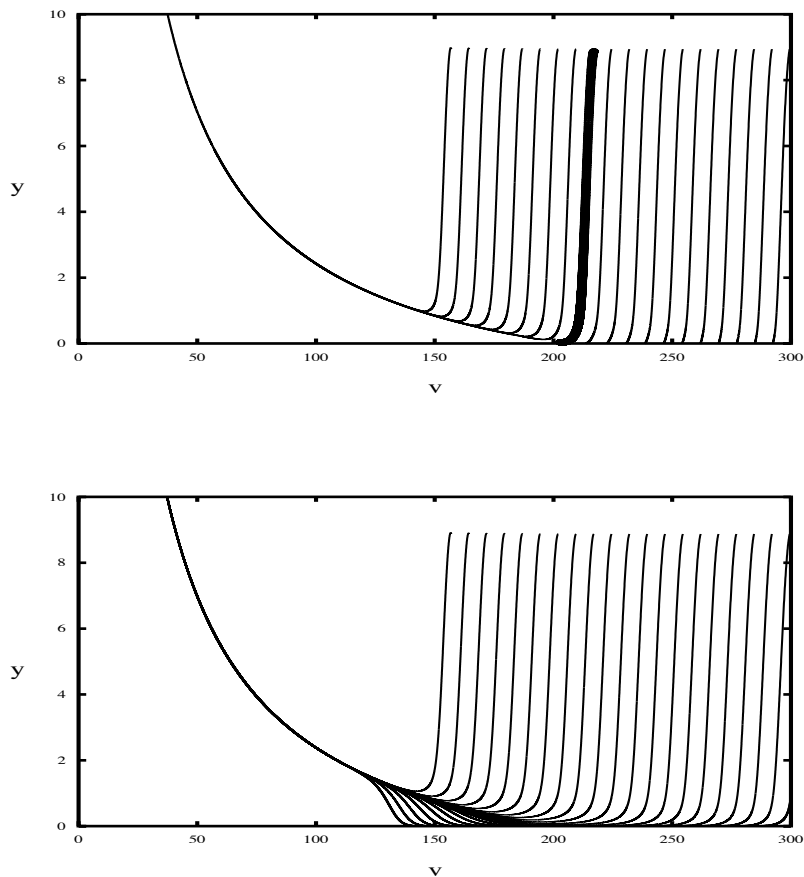


Figure 2: Top: The projection onto the  $v - y$  plane of a collection of orbits in the singular case  $\alpha = \omega = 0$ . Initial values  $v(0)$  range between 155 and 305,  $y(0) = 9$ , and  $x(0) = 0$ . The orbit singled out by the heavy line lies on the separatrix between two basins of attraction. Points to the left are attracted to the equilibrium  $(K, 0, 0)$  (therapeutic failure), and points to the right are attracted to the line of fixed points  $L$  (successful therapy). Other parameters are chosen as  $r = 0.206$ ,  $\rho = 0.2145$ ,  $K = 2139$ ,  $\varepsilon = 1.649$ ,  $\kappa = 0.001$ ,  $\delta = 0.5115$ . Bottom: The same simulation with  $\alpha = \omega = 0.001$ . As discussed in Section 5, the line  $L$  is no longer attracting.

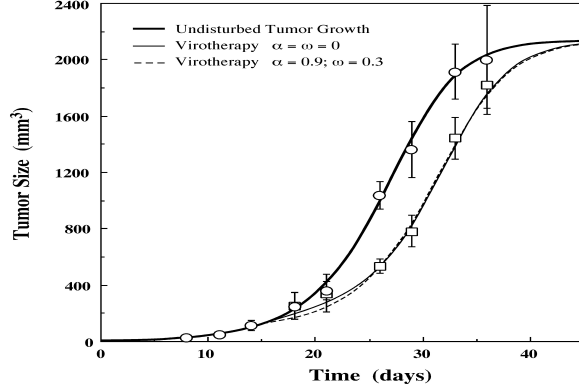


Figure 3: Weighted least-squares fitting of the model (3) to growth data for multiple myeloma in SCID mice [29]. Error bars with circles denote data for untreated tumor and with squares for tumor under virotherapy. Untreated tumor data were fitted ([12]) using the generalized logistic model (2) resulting in  $r = 0.2062134 \text{ day}^{-1}$ ,  $K = 2139.258$ ,  $\varepsilon = 1.648773$ . The values of parameters obtained by fitting to virotherapy data are given in Table 1, fits a) and c). For these fits we assumed that the tumor size at the start of virotherapy on day 15 was given by the model curve for the untreated tumor, i.e.  $y_0 = 126.237$ . The virus dose was  $v_0 = 2$ .

In the case of virotherapy, we fitted  $u(t) = x(t) + y(t)$  to data. The tumor size at the beginning of therapy,  $y_0$ , was obtained from the best-fit growth curve for the untreated tumor. The values of parameters  $r, K, \varepsilon$ , are those obtained by fitting to the untreated tumor (Fig. 3, also see [12]). The initial viral dose  $v_0$  was known from the experiment. The best fit was obtained when the lower limit for the allowed values of parameters  $\alpha$  and  $\omega$  was set to zero (Fig. 3) and the fit resulted in zero values. In terms of underlying biology one cannot completely exclude production of free virus and its elimination. However, some *in vivo* experiments ([28, 31]) suggest that the free virus population is not detectable, so one can infer that  $\alpha$  is very small.

The results of our fitting suggest that the existing 6 data points are insufficient to determine all five model parameters; specifically  $\alpha$  and  $\omega$  appear to be the most undetermined. Thus, for example, when we chose the lower limits  $\alpha = 0.9 \text{ day}^{-1}$ ,  $\omega = 0.3 \text{ day}^{-1}$  in the range of allowable parameter values, the minimization yielded those lower limits. The corresponding best fit curve passes through error bars of data points and can possibly be considered consistent with data, although  $\chi^2$  is larger (see Table 1). We have chosen a lower limit for  $\omega$  of  $0.3 \text{ day}^{-1}$ , because some *in vitro* experiments suggest that approximately 1/3 of virus particles are inactivated per day [49]. A lower limit for  $\alpha$  was chosen at  $0.9 \text{ day}^{-1}$  because if  $\alpha > 0.9 \text{ day}^{-1}$  and  $\omega = 0.3 \text{ day}^{-1}$  the best fit curve no longer passes through the error bars, and we can consider those fits inconsistent with data.

When the values for  $\alpha$  and  $\omega$  are changed, the fits suggest that other parameters do not change dramatically (see Table 1). Thus, if we do the fitting with  $\alpha$  and  $\omega$  limited from below to some acceptable values, we can obtain the values of other parameters. For the sake

fit	$\kappa$	$\delta$	$\alpha$	$\omega$	$\rho$	$\chi^2$
<i>a</i>	0.0009590090	0.5115017	0	0	0.2145849	1.01547
<i>b</i>	0.0009592272	0.5140769	0.001	0.0001	0.2153509	1.01657
<i>c</i>	0.0005911312	1.1189519	0.9	0.3	0.141120	1.84888

Table 1: Values of model rate constants (in day<sup>-1</sup>) obtained by fitting to virotherapy data (see Fig. 3). The last column presents the obtained  $\chi^2$ .

of exploring this model by numerical simulations, we chose the values for  $\alpha$  and  $\omega$  as a) the limiting case when they are zero, b) small but not zero, (suggested by in vivo experiments [28, 31]) and low  $\chi^2$ ), and c) as large as the data allows (see discussion above).

Although based on the existing experimental data we cannot determine model parameters accurately, model (3) is validated. This is not the case for the simplified model (4) which yielded completely unacceptable fits.

## 5 Simulations

As discussed in Section 3 equilibria are important for the virotherapy outcome. However, since significant therapeutic effects have to be achieved in a finite time period (1000 days for the mice considered above), it is necessary to investigate the predictions of model (3) by numerical simulations. Therefore, in the following we discuss results of numerical simulations chosen to demonstrate significant implications for the effects of virotherapy. Throughout this section we will use the parameters given in Table 1, and all quantities will be measured in the units discussed in the previous section. We will start with a discussion of the singular and singularly perturbed models corresponding to fits (a) and (b) respectively, in Table 1.

Fig. 4 shows the time profile for the total tumor burden  $u$ , as well as the populations of infected cells and the virus ( $x$  and  $v$  respectively). As was shown in Fig. 2, if the initial dose of virus is too low, the system rapidly approaches the equilibrium  $(K, 0, 0)$  corresponding to therapeutic failure. This is illustrated in Fig. 4a with an initial virus dose of  $v(0) = 10$ . There is a sharp initial increase in the number of infected tumor cells  $x(t)$  followed by a decrease in the total tumor size  $u(t) = y(t) + x(t)$ . However, as the viral load and the number of infected cells decrease, the tumor rebounds, increasing to the level of carrying capacity.

With an initial virus dose of  $v(0) = 226$  the tumor drops below the clinically detectable level  $u = 1$  at  $t = 6.54$ , and is still undetectable at  $t = 1000$  where  $u(1000) = 0.88$  (see Fig. 4b). Here  $v(0) \approx 226$  is the minimum level of initial virus needed for successful therapy. In particular, if  $v(0) = 225$ , then  $u(1000) > 1$ .

Note that therapy can be successful even if the initial condition  $(y(0), 0, v(0))$  is in the basin of attraction of the equilibrium  $(K, 0, 0)$ , as long as the tumor load remains undetectable up to time  $t = 1000$ . In fact, if continued, the orbit shown in Fig. 4b approaches  $(K, 0, 0)$  as  $t \rightarrow \infty$ . If the initial dose of virus is increased further to  $v(0) = 236$  virotherapy

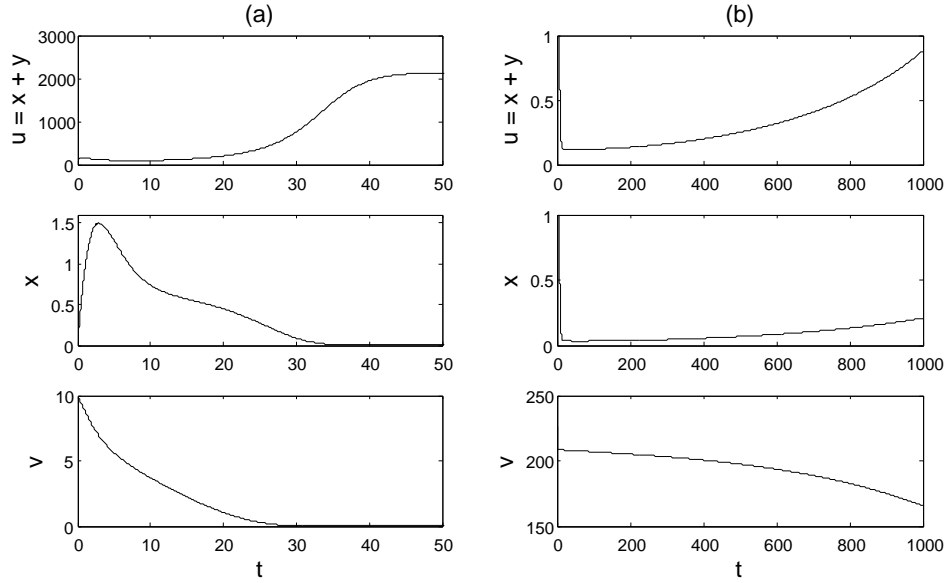


Figure 4: (a) Prediction of model (3) with an initial virus dose of  $v(0) = 10$ . Parameter values for  $r$ ,  $K$  and  $\varepsilon$  are the same as in Fig. 3, and  $(y(0), x(0)) = (126.237, 0)$ . The remaining parameters  $(\kappa, \delta, \alpha, \omega, \rho)$  are from the fit a) of Table 1. (b) A higher dose of initial virus leads to therapeutic success (see text).

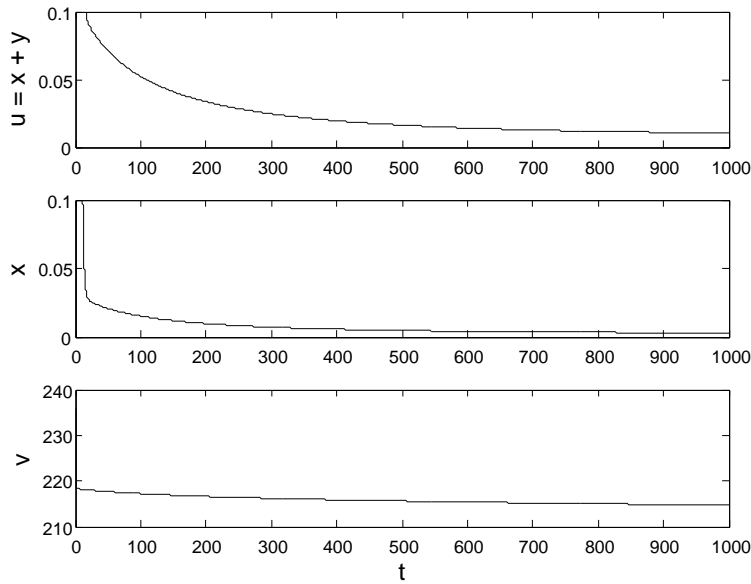


Figure 5: With an initial virus dose of  $v(0) = 236$  the tumor size drops below the clinically detectable level  $u = 1$  at  $t = 6.50$ , and is still decreasing at  $t = 1000$ , when  $u(1000) = 0.01$ . Conversely, if  $v(0) = 235$ , the tumor is undetectable but increasing at  $t = 1000$ . Parameter values are the same as in Fig. 4.

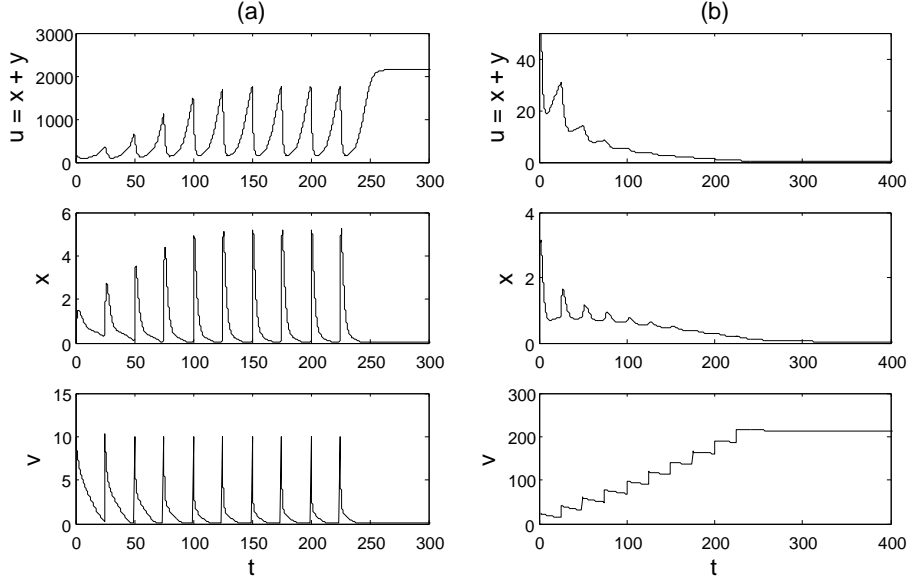


Figure 6: (a) The effect of administering ten doses of  $v_{dose} = 10$  units of virus every 25 days. (b) The effect of administering ten doses of  $v_{dose} = 29$  units of virus every 25 days. Parameter values are the same as Fig. 4.

is not only successful, but the initial point is in the basin of attraction of the line  $L$ . In this case the tumor is decreasing at time  $t = 1000$  and keeps decreasing if the simulation is continued (see Fig. 5).

Figure 6 illustrates the effect of administering the virus in several doses, rather than at once. Fig. 6(a) shows the effect of ten doses of virus, such that each dose corresponds to  $v_{dose} = 10$ . The doses are administered every 25 days, so that the total viral load does not increase over time. Each individual dose temporarily reduces the tumor size but the dosing schedule does not lead to long term tumor eradication.

Similarly, Fig. 6b shows the effect of ten doses of  $v_{dose} = 29$  units of virus each, scheduled every 25 days. In this case, the tumor is undetectable when  $t = 1000$  ( $u(1000) < 1$ ). The number of doses and the time period between them does not determine whether therapy will ultimately be successful or not. In general, for a fixed initial tumor size  $y(0)$ , the viral load must reach a certain minimal value for the therapy to be a success. This is analogous to the results in Fig. 9 and 10 where we show which initial conditions lead to a successful therapy and which do not (we discuss these figures in detail below).

The growth rate  $r$  has a large effect on the outcome of therapy. Tumor growth can be slowed down by the use of inhibitors of DNA synthesis so that  $r$  can be significantly reduced. As an example, we consider  $r$  equal to 1% of the fit a) value and find that  $v(0) = 12$  is sufficient for the tumor to be undetectable at  $t = 1000$  ( $u(1000) < 1$ ). Thus, as the rate of tumor cell replication is slowed down, the total dose of virus necessary to control the tumor decreases. However, with the smaller virus load it takes much longer for the tumor to shrink in size, specifically,  $u(687.08) = 1$ .

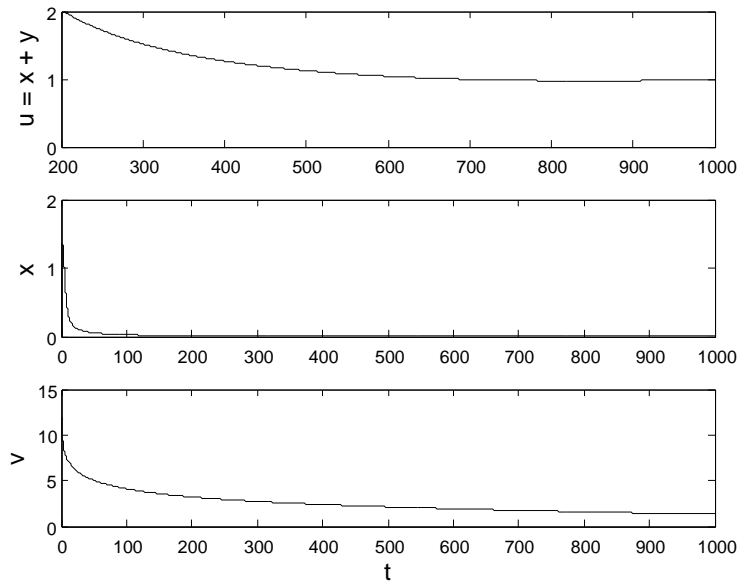


Figure 7: Decreasing the growth rate  $r$  has a large effect on the success of therapy. If  $r$  is decreased by two orders of magnitude compared to Fig. 4 the dose of virus sufficient for successful therapy is reduced to  $v(0) = 12$ .

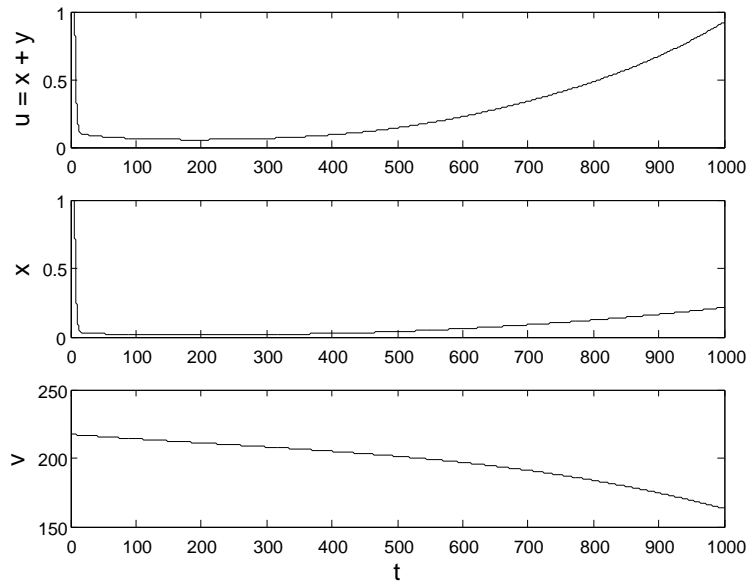


Figure 8: The behavior of the singularly perturbed system ( $\alpha \neq 0$  and  $\omega \neq 0$ ) is similar to that of the singular system. Compare with Fig. 4b. Parameters are chosen according to fit b) in Table 1.

We next consider the effect of small, but nonzero virus production ( $\alpha \neq 0$ ) and elimination ( $\omega \neq 0$ ) using the parameter values from fit b) in Table 1. Compared to the simulation results in Fig. 4b, it is somewhat more difficult to achieve successful therapy requiring  $v(0) = 235.0$  with  $u(1000) = 0.92$  and  $u = 1$  when  $t = 6.48$ . Other qualitative behavior regarding multiple doses and decreasing  $r$  are also the same for the parameters in fit b), as in fit a). On the other hand, increasing  $\alpha$  relative to  $\omega$ , and hence increasing the viral load can lead to a successful result. This is because the relatively large rate of virus production ultimately leads to a large viral load; this is analogous to the large initial viral load  $v(0)$  when using parameters from fit a). We can therefore conclude that the behavior of the singularly perturbed model, is very similar to that of the singular model.

In Fig. 9 we examine the effect of the initial tumor size on the final outcome of virotherapy. The shades of gray indicate the final tumor size  $u(1000)$  as a function of the initial conditions  $(y(0), 0, v(0))$ . Of particular note is that it is sometimes preferable to allow the tumor to grow to a larger size before administering the virus. For example, for a fixed viral load of  $v(0) = 210$ , if the initial tumor size is  $y(0) = 1600$ , then therapy fails. On the other hand, if the tumor is larger with  $y(0) = 1900$ , then not only is the tumor undetectable at  $t = 1000$ , but it is essentially eliminated with  $u(1000) = O(10^{-6})$ . A potential explanation for this may be that a higher tumor burden at the time of virus administration increases the number of cells that are infected, leading to a higher population of tumor cells that can fuse with surrounding cells ( $\rho$ ) and produce additional virus particles ( $\alpha$ ).

In Fig. 9 we also observe an “island” of initial conditions where virus therapy is unsuccessful, which is surrounded by initial conditions that lead to success,  $u(1000) < 1$ . We do not currently have an explanation for why this isolated region exists.

In Fig. 10 we again consider the state of the system at  $t = 1000$  but with the tumor growth rate  $r$  reduced by a factor of ten. As noted in Fig. 7 when  $r$  is reduced, a lower initial dose of virus is needed to achieve successful therapy; the curve where  $u(1000) = 1$  has shifted to much lower values of  $v(0)$ . In addition, the sharp upper boundary between  $u(1000) = O(10^3)$  (black) and  $O(10^{-6})$  (white) that exists in Fig. 9 has shifted upward to higher values of  $u$ , much larger than the level of saturation, and does not appear in the figure.

Based on (3), one would expect that as the ability of infected cells to fuse with uninfected tumor cells ( $\rho$ ) increases, the tumor burden  $u(1000)$  and  $y(1000)$  should decrease. Therefore, the results in Fig. 11 appear counterintuitive. The increase in  $u(1000)$ , though, is not of great significance for the therapy if  $\rho > 0.2$ , where 0.2 is approximately the value for  $\rho$  obtained by fitting (see Table 1). We found that the equilibrium value  $x_3$  (see (9)) slightly decreases with  $\rho$  while, of course,  $y_3$  is constant. However at the time  $t = 1000$  we are still very far from the equilibrium and the behavior is as shown in Fig. 11. Otherwise, when  $\alpha$  is much smaller than 0.6 and  $\rho$  sufficiently large so that the tumor burden achieves a minimum before growing to the level of carrying capacity, this minimal tumor burden indeed decreases with  $\rho$ . However the effect is quite insignificant for  $\rho$  smaller than 1.5. It is unlikely that values of  $\rho$  higher than 1.5 are realistic.

Finally, in Fig. 12 we show that Eqs. (3) support damped oscillatory behavior. Fig. 12a

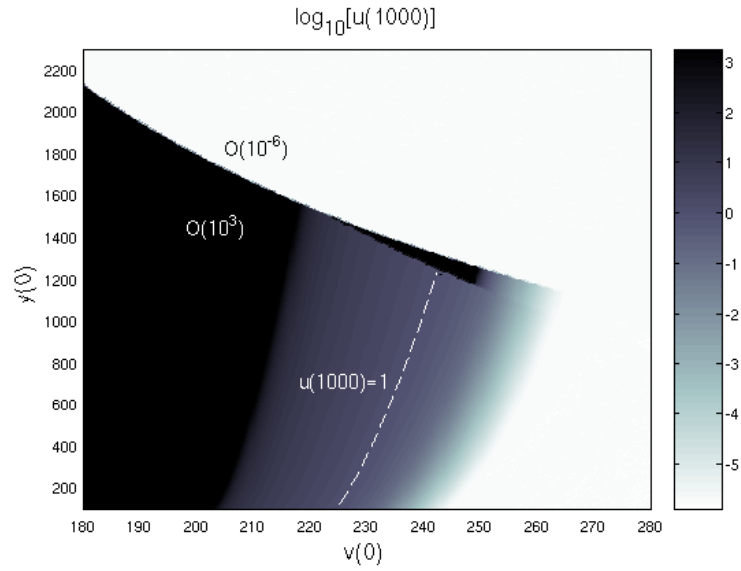


Figure 9: The total tumor size  $u = y + x$  at  $t = 1000$  as a function of the initial viral load  $v(0)$  and the initial tumor size  $y(0)$  using the parameters from fit a). The black region corresponds to initial conditions that lead to unsuccessful therapy such that  $u(1000)$  has reached the level of the carrying capacity. The white region corresponds to very successful therapy such that the tumor is almost eradicated with  $u(1000) = O(10^{-6})$ . The dashed curve identifies when the tumor is undetectable with  $u(1000) = 1$ .

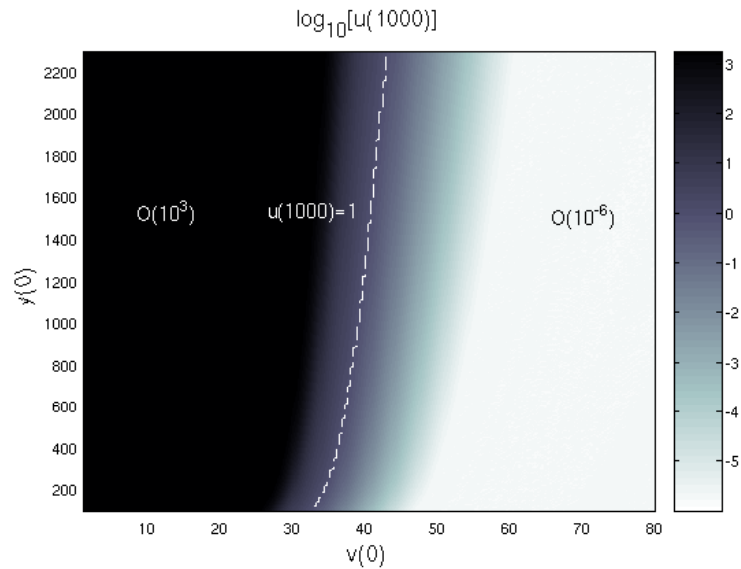


Figure 10: Same as Fig. 9 but with the tumor growth rate  $r$  reduced by a factor of 10 ( $r = 0.02062134$ ).

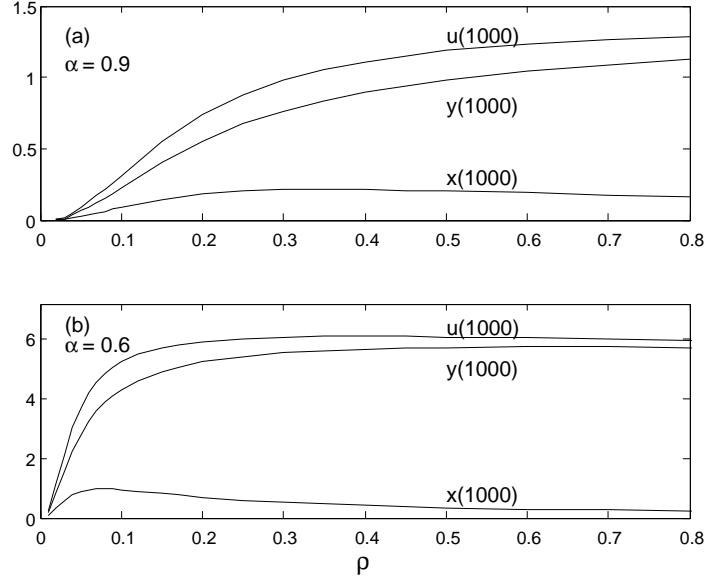


Figure 11: The size of the tumor at  $t = 1000$  as a function of the cell fusion rate  $\rho$ . Other parameters are those of fit b) with (a)  $\alpha = 0.9$  and (b)  $\alpha = 0.6$ . In each figure there is a value of  $\rho$  such that the number of infected tumor cells  $x(1000)$  is maximal. For further increases in  $\rho$ ,  $x(1000)$  decreases. However, in (a) the total tumor size  $u(1000)$  and the uninfected tumor size  $y(1000)$  are still increasing, while in (b) they are slightly decreasing.

shows strongly damped oscillations for parameter values similar to those of fit b). Only a single maximum of  $u$  is visible given the scale but the corresponding numerical data clearly exhibit very small amplitude oscillations. Fig.12b shows more dramatic oscillations but for parameter values away from those given in Table 1.

## 6 Conclusion

The availability of novel therapeutic agents such a replicating viruses for cancer therapy introduces a new paradigm in the therapy of these diseases. Therapeutic success depends on the highly specific interaction between the oncolytic virus and the tumor cell population with the dynamic considerations determining the outcome. We have presented a model to try and understand different aspects of the effect of therapy with attenuated measles viruses on tumor growth. In particular, we are able to provide partial answers to the questions posed in the Introduction.

- 1) The initial tumor burden is important, but not crucial for the outcome of therapy. Contrary to intuition, a larger initial tumor burden may facilitate therapy under certain conditions, perhaps by increasing the efficiency of virus-tumor cell interactions. The result is a higher pool of infected tumor cells that proceed to generate new virus

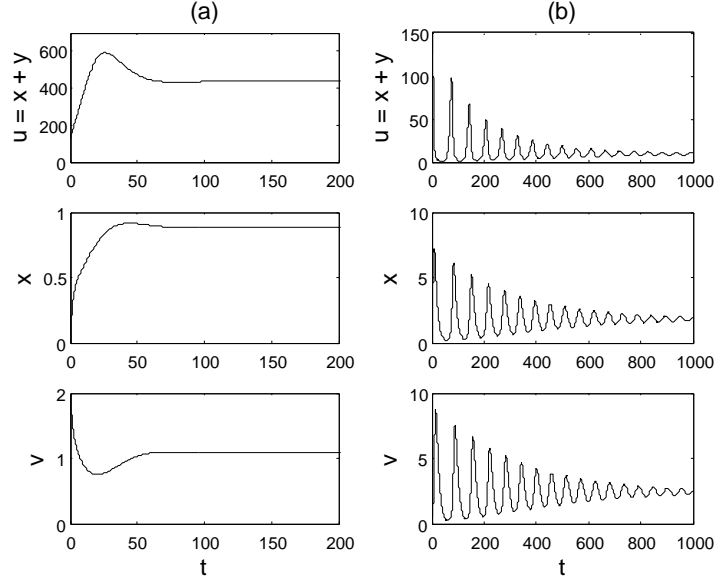


Figure 12: (a) Strongly-damped oscillations using fit b) parameters with  $\alpha = 0.6$  and  $\omega = 0.07$ . (b) Weakly-damped oscillations using  $\kappa = 0.01$ ,  $\rho = 0.1$ ,  $\delta = 0.1$ ,  $\alpha = 0.5$  and  $\omega = 0.3$ .

particles and fuse surrounding tumor cells stopping their replication and ultimately leading to their death.

- 2) It is not possible to cure the experimentally tested tumor xenografts with a therapeutically achievable dose of virus. Our analysis suggests that 226 million virus particles must be injected for the virus alone to eradicate the tumor. This is not possible in a mouse unless the virus can be concentrated significantly without loss of titer. However, if tumor growth can be slowed, the virus requirements decrease significantly and are achievable with current technology. Such an approach may offer also an additional margin of safety since the total dose of virus that will need to be injected is small and hence the risk of adverse effects will be expected to decrease.
- 3) If optimal virus therapy is defined as the smallest effective dose of virus that can operationally control the tumor for the lifetime of the animal, then combining virotherapy with strategies to slow tumor growth can significantly reduce the demands on the virus load needed for cure.
- 4) Dose scheduling does not seem to play an important role on the outcome of therapy. The main determinant of the therapeutic outcome is the total dose of virus that can be administered.

**Acknowledgment:** This research has been supported by NSF grants DMS-0244529 and DMS-0604229, and a Texas ARP/ATP grant to KJ. ŽB acknowledges support from Grant CA-100634 and from Mayo Clinic Cancer Center Support grant CA15083 funded by the NIH. DD is supported by the Mayo Foundation.

## References

- [1] R. A. Kyle and S. V. Rajkumar. Multiple myeloma. *N Engl J Med*, 351(18):1860–73, 2004.
- [2] D. Kirn, R. L. Martuza, and J. Zwiebel. Replication-selective virotherapy for cancer: Biological principles, risk management and future directions. *Nat Med*, 7(7):781–7, 2001.
- [3] S. J. Russell. RNA viruses as virotherapy agents. *Cancer Gene Ther*, 9(12):961–6, 2002.
- [4] J. Nemunaitis, F. Khuri, I. Ganly, J. Arseneau, M. Posner, E. Vokes, J. Kuhn, T. McCarty, S. Landers, A. Blackburn, L. Romel, B. Randlev, S. Kaye, and D. Kirn. Phase ii trial of intratumoral administration of onyx-015, a replication-selective adenovirus, in patients with refractory head and neck cancer. *J Clin Oncol*, 19(2):289–98, 2001.
- [5] T. Reid, E. Galanis, J. Abbruzzese, D. Sze, J. Andrews, L. Romel, M. Hatfield, J. Rubin, and D. Kirn. Intra-arterial administration of a replication-selective adenovirus (dl1520) in patients with colorectal carcinoma metastatic to the liver: a phase i trial. *Gene Ther*, 8(21):1618–26, 2001.
- [6] T. Reid, E. Galanis, J. Abbruzzese, D. Sze, L. M. Wein, J. Andrews, B. Randlev, C. Heise, M. Uprichard, M. Hatfield, L. Rome, J. Rubin, and D. Kirn. Hepatic arterial infusion of a replication-selective oncolytic adenovirus (dl1520): phase ii viral, immunologic, and clinical endpoints. *Cancer Res*, 62(21):6070–9, 2002.
- [7] A. L. Pecora, N. Rizvi, G. I. Cohen, N. J. Meropol, D. Stermann, J. L. Marshall, S. Goldberg, P. Gross, J. D. O’Neil, W. S. Groene, M. S. Roberts, H. Rabin, M. K. Bamat, and R. M. Lorence. Phase i trial of intravenous administration of pv701, an oncolytic virus, in patients with advanced solid cancers. *J Clin Oncol*, 20(9):2251–66, 2002.
- [8] D. Wodarz. Viruses as antitumor weapons: defining conditions for tumor remission. *Cancer Res*, 61(8):3501–7, 2001.
- [9] D. Wodarz. Gene therapy for killing p53-negative cancer cells: use of replicating versus nonreplicating agents. *Hum Gene Ther*, 14(2):153–9, 2003.
- [10] J. T. Wu, H. M. Byrne, D. H. Kirn, and L. M. Wein. Modeling and analysis of a virus that replicates selectively in tumor cells. *Bull Math Biol*, 63(4):731–68, 2001.
- [11] J. T. Wu, D. H. Kirn, and L. M. Wein. Analysis of a three-way race between tumor growth, a replication-competent virus and an immune response. *Bull Math Biol*, 66(4):605–25, 2004.
- [12] D. Dingli, M. D. Cascino, K. Josić, S. J. Russell, and Ž. Bajzer. Mathematical modeling of cancer radiovirotherapy. *Math Biosci*, 199(1):55–78, 2006.

- [13] D. Grote, S. J. Russell, T. I. Cornu, R. Cattaneo, R. Vile, G. A. Poland, and A. K. Fielding. Live attenuated measles virus induces regression of human lymphoma xenografts in immunodeficient mice. *Blood*, 97(12):3746–54, 2001.
- [14] K. W. Peng, G. J. Ahmann, L. Pham, P. R. Greipp, R. Cattaneo, and S. J. Russell. Systemic therapy of myeloma xenografts by an attenuated measles virus. *Blood*, 98(7):2002–7, 2001.
- [15] K. W. Peng, C. J. TenEyck, E. Galanis, K. R. Kalli, L. C. Hartmann, and S. J. Russell. Intraperitoneal therapy of ovarian cancer using an engineered measles virus. *Cancer Res*, 62(16):4656–62, 2002.
- [16] L. K. Phuong, C. Allen, K. W. Peng, C. Giannini, S. Greiner, C. J. TenEyck, P. K. Mishra, S. I. Macura, S. J. Russell, and E. C. Galanis. Use of a vaccine strain of measles virus genetically engineered to produce carcinoembryonic antigen as a novel therapeutic agent against glioblastoma multiforme. *Cancer Res*, 63(10):2462–9, 2003.
- [17] C. J. McDonald, C. Erlichman, J. N. Ingle, G. A. Rosales, C. Allen, S. M. Greiner, M. E. Harvey, P. J. Zollman, S. J. Russell, and E. Galanis. A measles virus vaccine strain derivative as a novel oncolytic agent against breast cancer. *Breast Cancer Res Treat*, 99(2):177–84, 2006.
- [18] U. Schneider, V. von Messling, P. Devaux, and R. Cattaneo. Efficiency of measles virus entry and dissemination through different receptors. *J Virol*, 76(15):7460–7, 2002.
- [19] B. D. Anderson, T. Nakamura, S. J. Russell, and K. W. Peng. High cd46 receptor density determines preferential killing of tumor cells by oncolytic measles virus. *Cancer Res*, 64(14):4919–26, 2004.
- [20] H. T. Ong, M. M. Timm, P. R. Greipp, T. E. Witzig, A. Dispenzieri, S. J. Russell, and K. W. Peng. Oncolytic measles virus targets high cd46 expression on multiple myeloma cells. *Exp Hematol*, 34(6):713–20, 2006.
- [21] K. W. Peng, K. A. Donovan, U. Schneider, R. Cattaneo, J. A. Lust, and S. J. Russell. Oncolytic measles viruses displaying a single-chain antibody against cd38, a myeloma cell marker. *Blood*, 101(7):2557–62, 2003.
- [22] A. D. Bucheit, S. Kumar, D. M. Grote, Y. Lin, V. von Messling, R. B. Cattaneo, and A. K. Fielding. An oncolytic measles virus engineered to enter cells through the cd20 antigen. *Mol Ther*, 7(1):62–72, 2003.
- [23] U. Schneider, F. Bullough, S. Vongpunsawad, S. J. Russell, and R. Cattaneo. Recombinant measles viruses efficiently entering cells through targeted receptors. *J Virol*, 74(21):9928–36, 2000.

- [24] A. L. Hammond, R. K. Plemper, J. Zhang, U. Schneider, S. J. Russell, and R. Cattaneo. Single-chain antibody displayed on a recombinant measles virus confers entry through the tumor-associated carcinoembryonic antigen. *J Virol*, 75(5):2087–96, 2001.
- [25] T. Nakamura, K. W. Peng, S. Vongpunsawad, M. Harvey, H. Mizuguchi, T. Hayakawa, R. Cattaneo, and S. J. Russell. Antibody-targeted cell fusion. *Nat Biotechnol*, 22(3):331–6, 2004.
- [26] T. Nakamura, K. W. Peng, M. Harvey, S. Greiner, I. A. Lorimer, C. D. James, and S. J. Russell. Rescue and propagation of fully retargeted oncolytic measles viruses. *Nat Biotechnol*, 23(2):209–14, 2005.
- [27] E. M. Hadac, K. W. Peng, T. Nakamura, and S. J. Russell. Reengineering paramyxovirus tropism. *Virology*, 329(2):217–25, 2004.
- [28] K. W. Peng, S. Fecteau, T. Wegman, D. O’Kane, and S. J. Russell. Non-invasive in vivo monitoring of trackable viruses expressing soluble marker peptides. *Nat Med*, 8(5):527–31, 2002.
- [29] D. Dingli, K. W. Peng, M. E. Harvey, P. R. Greipp, M. K. O’Connor, R. Cattaneo, J. C. Morris, and S. J. Russell. Image-guided radiovirotherapy for multiple myeloma using a recombinant measles virus expressing the thyroidal sodium iodide symporter. *Blood*, 103(5):1641–6, 2004.
- [30] D. Dingli, B. J. Kemp, M. K. O’Connor, J. C. Morris, S. J. Russell, and V. J. Lowe. Combined I-124 positron emission tomography/computed tomography imaging of nis gene expression in animal models of stably transfected and intravenously transfected tumor. *Mol Imaging Biol*, 8(1):16–23, 2006. 1536-1632.
- [31] K. W. Peng, E. M. Hadac, B. D. Anderson, R. Myers, M. Harvey, S. M. Greiner, D. Soeffker, M. J. Federspiel, and S. J. Russell. Pharmacokinetics of oncolytic measles virotherapy: eventual equilibrium between virus and tumor in an ovarian cancer xenograft model. *Cancer Gene Ther*, 13(8):732–8, 2006.
- [32] Y. Tao and Q. Guo. The competitive dynamics between tumor cells, a replication-competent virus and an immune response. *J Math Biol*, 51(1):37–74, 2005.
- [33] L. M. Wein, J. T. Wu, and D. H. Kirn. Validation and analysis of a mathematical model of a replication-competent oncolytic virus for cancer treatment: implications for virus design and delivery. *Cancer Res*, 63(6):1317–24, 2003.
- [34] D. Dingli, S. J. Russell, and J. C. Morris. In vivo imaging and tumor therapy with the sodium iodide symporter. *J Cell Biochem*, 90(6):1079–86, 2003.
- [35] D. Dingli, R. M. Diaz, E. R. Bergert, M. K. O’Connor, J. C. Morris, and S. J. Russell. Genetically targeted radiotherapy for multiple myeloma. *Blood*, 102(2):489–96, 2003.

- [36] A. S. Novozhilov, F. S. Berezovskaya, E. V. Koonin, and G. P. Karev. Mathematical modeling of tumor therapy with oncolytic viruses: regimes with complete tumor elimination within the framework of deterministic models. *Biol Direct*, 1:6, 2006.
- [37] M. Marušić, Ž. Bajzer, S. Vuk-Pavlović, and J. P. Freyer. Tumor growth in vivo and as multicellular spheroids compared by mathematical models. *Bull Math Biol*, 56(4):617–631, 1994.
- [38] Ž. Bajzer, S. Vuk-Pavlović, and M. Huzak. Mathematical modeling of tumor growth kinetics. In J.A. Adam and N. Bellomo, editors, *A Survey of Models for Tumor-immune System Dynamics*, chapter 3, pages 89–133. Birkhäuser, 1997.
- [39] D. A. Cameron, A. A. Ritchie, and W. R. Miller. The relative importance of proliferation and cell death in breast cancer growth and response to tamoxifen. *Eur J Cancer*, 37(12):1545–1553, 2001.
- [40] R Chignola, A Schenetti, G Andrighetto, E Chiesa, R Foroni, S Sartoris, G Tridente, and D Liberati. Forecasting the growth of multicell tumour spheroids: implications for the dynamic growth of solid tumours. *Cell Prolif*, 33(4):219–229, 2000.
- [41] J A Spratt, D von Fournier, J S Spratt, and E E Weber. Decelerating growth and human breast cancer. *Cancer*, 71(6):2013–2019, 1993.
- [42] H. M. Byrne. Modelling avascular tumour growth. In L. Preziosi, editor, *Cancer Modelling and Simulation*, chapter 4, pages 75–120. CRC Press, 2003.
- [43] Ž. Bajzer, M. Marušić, and S. Vuk-Pavlović. Conceptual frameworks for mathematical modeling of tumor growth dynamics. *Mathl Comput Modelling*, 23:31–46, 1996.
- [44] R. I. Fletcher. A general solution for the complete richards function. *Math Biosci*, 27:349–360, 1975.
- [45] J. Heaney, T. Barrett, and S. L. Cosby. Inhibition of in vitro leukocyte proliferation by morbilliviruses. *J Virol*, 76(7):3579–3584, 2002.
- [46] D. Wodarz and N.L. Komarova. *Computational Biology of Cancer: Lecture Notes and Mathematical Modeling*. World Scientific Publishing Company, 2005.
- [47] A. Hurwitz. On the conditions under which an equation has only roots with negative real parts. In R. Bellman and R. Kalaba, editors, *Selected Papers on Mathematical Trends in Control Theory*. Dover, New York, 1964.
- [48] C. Offord and Ž. Bajzer. A hybrid global optimization algorithm involving simplex and inductive search. *Lecture Notes Comput Sci*, 2074:680–688, 2006.
- [49] T. Whistler, W. J. Bellini, and P. A. Rota. Generation of defective interfering particles by two vaccine strains of measles virus. *Virology*, 220(2):480–4, 1996.